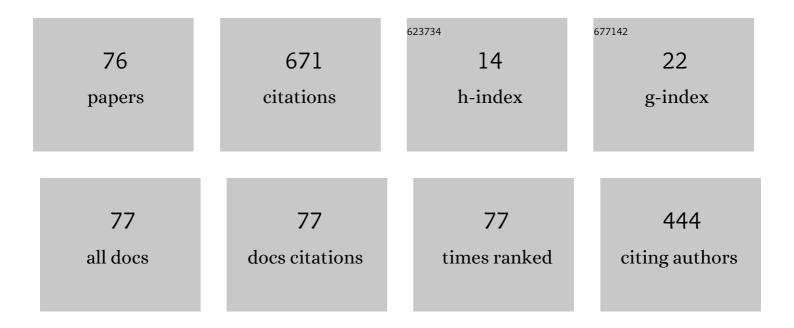
## Jiamin Yang

List of Publications by Year in descending order

Source: https://exaly.com/author-pdf/7077518/publications.pdf Version: 2024-02-01



#	Article	IF	CITATIONS
1	Theoretical investigations on x-ray transport in radiation transport experiments on the Shenguang-III prototype laser facility. Matter and Radiation at Extremes, 2022, 7, 025901.	3.9	4
2	Measurement of Time-Dependent Drive Flux on the Capsule for Indirectly Driven Inertial Confinement Fusion Experiments. Physical Review Letters, 2022, 128, 075001.	7.8	2
3	Giant retardation effect in electron-electron interaction. Physical Review A, 2022, 105, .	2.5	6
4	An estimation method of the spatial resolution for magnifying fast neutron radiography. AIP Advances, 2022, 12, 055117.	1.3	3
5	Intense Electromagnetic Pulses Generated From kJ-Laser Interacting With Hohlraum Targets. IEEE Transactions on Nuclear Science, 2022, 69, 2027-2036.	2.0	2
6	Solutions of several theory and technique problems in high-space-resolving hotspot electron temperature diagnosis techniques in inertial confinement fusion. AIP Advances, 2022, 12, 075007.	1.3	0
7	Experimental and simulation studies of thermal transport based on plasma flow motion in laser-ablated dense regions of Au and CH. Matter and Radiation at Extremes, 2022, 7, .	3.9	3
8	Optimization of x-ray emissions with Gd + Au + Gd sandwich design. AlP Advances, 2021, 11, 025005.	1.3	1
9	Early-time symmetry quantifying with thin-shell capsule radiography for pulse shaped implosion. Physics of Plasmas, 2021, 28, 032711.	1.9	1
10	Studies of laser-plasma interaction physics with low-density targets for direct-drive inertial confinement fusion on the Shenguang III prototype. Matter and Radiation at Extremes, 2021, 6, .	3.9	31
11	Multi-keV x-ray radiator from titanium cylindrical cavity at the Shenguang-III prototype laser facility. Physics of Plasmas, 2021, 28, .	1.9	3
12	Quantitative observation of monochromatic X-rays emitted from implosion hotspot in high spatial resolution in inertial confinement fusion. Scientific Reports, 2021, 11, 14492.	3.3	4
13	Anisotropy and polarization of x-ray line emissions in the dielectronic recombination of hydrogenlike Fe25+ ions. Physical Review A, 2021, 104, .	2.5	5
14	Sound Velocity Measurement of Shock-Compressed Quartz at Extreme Conditions. Minerals (Basel,) Tj ETQq0 0	0 rgBT /Ov	verlock 10 Tf
15	First Inertial Confinement Fusion Implosion Experiment in Octahedral Spherical Hohlraum. Physical Review Letters, 2021, 127, 245001.	7.8	16
16	Transparency measurement of lithium fluoride under laser-driven accelerating shock loading. Journal of Applied Physics, 2020, 128, .	2.5	5
17	Chunk mixing implosion experiments using deuterated foam capsules with gold dopant. Physical Review E, 2020, 102, 023204.	2.1	2

18Recent diagnostic developments at the 100 kJ-level laser facility in China. Matter and Radiation at<br/>Extremes, 2020, 5, .3.925

Jiamin Yang

#	Article	IF	CITATIONS
19	Demonstration of bright x-ray sources from solid and foam TiO2 targets at the Shenguang-III prototype laser facility. AIP Advances, 2020, 10, .	1.3	2
20	Recent research progress of laser plasma interactions in Shenguang laser facilities. Matter and Radiation at Extremes, 2019, 4, .	3.9	28
21	First polar direct-drive exploding-pusher target experiments on the ShenGuang laser facility*. Chinese Physics B, 2019, 28, 095203.	1.4	4
22	Progress in optical Thomson scattering diagnostics for ICF gas-filled hohlraums. Matter and Radiation at Extremes, 2019, 4, .	3.9	10
23	Investigation on laser plasma instability of the outer ring beams on SGIII laser facility. AIP Advances, 2019, 9, .	1.3	6
24	Measurement of ionic structure in isochorically heated graphite from X-ray Thomson scattering. Physics of Plasmas, 2019, 26, 022702.	1.9	1
25	Measurement of P2 M-band flux asymmetry in indirect-drive hohlraum on Shenguang-III prototype laser facility. Review of Scientific Instruments, 2019, 90, 043505.	1.3	1
26	The effect of scattered neutrons on the ion temperature measurement with different line-of-sight on the SGIII laser facility. AIP Advances, 2019, 9, 015124.	1.3	1
27	Study of M-band X-ray preheating effect on shock propagation via streaked optical pyrometer system at SG-III prototype lasers. Physics of Plasmas, 2019, 26, .	1.9	7
28	First Octahedral Spherical Hohlraum Energetics Experiment at the SGIII Laser Facility. Physical Review Letters, 2018, 120, 165001.	7.8	16
29	Opacity measurements of a molybdenum plasma with open M-shell configurations. Physics of Plasmas, 2018, 25, 023301.	1.9	5
30	Mixing-rules calculations and AAMD simulations for EOSs of deuterium–xenon mixtures. Canadian Journal of Physics, 2018, 96, 1404-1408.	1.1	0
31	Efficient soft x-ray sources from laser-irradiated gold foam targets with well-controlled impurities. Nuclear Fusion, 2018, 58, 016038.	3.5	14
32	Experimental and simulation studies on radiative properties of uranium planar target coated with an ultrathin aluminum layer. Nuclear Fusion, 2018, 58, 026020.	3.5	3
33	Investigation of the yield degradation of the first shaped-pulse implosion experiments on the SG-III laser facility. Physics of Plasmas, 2018, 25, .	1.9	5
34	Energy Levels, Radiative Rates, and Lifetimes for Transitions in Fe XIV. Journal of Applied Spectroscopy, 2018, 85, 749-759.	0.7	3
35	Note: New method for high-space-resolving hotspot electron temperature measurements on Shenguang-III prototype. Review of Scientific Instruments, 2018, 89, 096108.	1.3	4
36	Implementation of ultraviolet Thomson scattering on SG-III laser facility. Review of Scientific Instruments, 2018, 89, 093505.	1.3	8

JIAMIN YANG

#	Article	IF	CITATIONS
37	A time-gated multi-channel x-ray crystal spectrometer on the Shenguang-III laser facility. Review of Scientific Instruments, 2018, 89, 083108.	1.3	0
38	Method to measure the temporal resolution of x-ray framing camera. Optical Engineering, 2018, 57, 1.	1.0	5
39	Comparing the soft x-rays transport in Si and Ge-sandwich targets by measuring transmission flux. Physics of Plasmas, 2017, 24, 032703.	1.9	0
40	Measurement of residual carbon in chamber of Shenguang II laser facility. Physics of Plasmas, 2017, 24, 072707.	1.9	3
41	Observation of an extremely-long-lived metastable level in a Ti-like system via an <mml:math xmlns:mml="http://www.w3.org/1998/Math/MathML"&gt;<mml:mi>L</mml:mi> -shell dielectronic recombination measurement in highly charged <mml:math xmlns:mml="http://www.w3.org/1998/Math/MathML"&gt;<mml:mrow><mml:mn>3</mml:mn><mml:msup><mn< td=""><td>2.5 nl:mi&gt;d</td></mn<><td>4 nl:mi&gt;<mml:n< td=""></mml:n<></td></mml:msup></mml:mrow></mml:math </mml:math 	2.5 nl:mi>d	4 nl:mi> <mml:n< td=""></mml:n<>
42	ions of tungsten. Physical Review A, 2017, 96, . Multiconfiguration Dirac–Fock calculation of Kα transition energies in beryllium like titanium. Indian Journal of Physics, 2017, 91, 1477-1485.	1.8	0
43	Transition properties of the Be-like \$\$hbox {K}alpha \$\$ K α X-ray from Mg IX. Pramana - Journal of Physics, 2017, 89, 1.	1.8	0
44	Experimental demonstration of laser to x-ray conversion enhancements with low density gold targets. Applied Physics Letters, 2016, 108, .	3.3	15
45	Fluorescence based imaging for M-band drive symmetry measurement in hohlraum. Physics of Plasmas, 2016, 23, .	1.9	4
46	Radiation flux study of spherical hohlraums at the SGIII prototype facility. Physics of Plasmas, 2016, 23, .	1.9	14
47	Design and experimental study of a secondary hohlraum radiation source with laser focal spots blocked. Physics of Plasmas, 2016, 23, .	1.9	2
48	Optimization of x-ray emission from under-critical CH foam coated gold targets by laser irradiation. Nuclear Fusion, 2016, 56, 086002.	3.5	8
49	Reducing wall plasma expansion with gold foam irradiated by laser. Physics of Plasmas, 2015, 22, .	1.9	13
50	The spectral lines of highly charged gold ions. Radiation Effects and Defects in Solids, 2015, 170, 138-143.	1.2	0
51	A K-shell model for laser-produced Al plasma. Radiation Effects and Defects in Solids, 2015, 170, 407-413.	1.2	3
52	Uranium hohlraum with an ultrathin uranium–nitride coating layer for low hard x-ray emission and high radiation temperature. New Journal of Physics, 2015, 17, 113004.	2.9	10
53	Spectroscopic studies of shell mix in directly driven implosion on SGIII prototype laser facility. Physics of Plasmas, 2014, 21, 122707.	1.9	4
54	The radiation temperature and <i>M</i> -band fraction inside hohlraum on the SGIII-prototype laser facility. Physics of Plasmas, 2014, 21, 022704.	1.9	10

Jiamin Yang

#	Article	IF	CITATIONS
55	Enhanced x-ray emissions from low-density high-Z mixture plasmas generated with intense nanosecond laser. Physics Letters, Section A: General, Atomic and Solid State Physics, 2014, 378, 813-816.	2.1	4
56	The M-band transmission flux of the plastic foil with a coated layer of silicon or germanium. Applied Physics Letters, 2014, 104, 054106.	3.3	10
57	Calibration of a gated flat field spectrometer as a function of x-ray intensity. Review of Scientific Instruments, 2014, 85, 043104.	1.3	5
58	Enhanced x-ray emissions from Au-Gd mixture targets ablated by a high-power nanosecond laser. Journal of Applied Physics, 2014, 115, 043305.	2.5	8
59	A simple method to verify the opacity and equation of state of high-Z plasmas. Physics of Plasmas, 2013, 20, .	1.9	8
60	Plasma effect on the <i>K</i> α group emission of He-like molybdenum. Radiation Effects and Defects in Solids, 2013, 168, 858-865.	1.2	3
61	The impact of low-Z impurities on x-ray conversion efficiency from laser-produced plasmas of low-density gold foam targets. Physics of Plasmas, 2013, 20, 123305.	1.9	12
62	Enhancement of laser to x-ray conversion with a low density gold target. Applied Physics Letters, 2013, 102, .	3.3	27
63	Detailed energy distributions in laser-produced plasmas of solid gold and foam gold planar targets. Physics of Plasmas, 2013, 20, .	1.9	14
64	Instantaneous x-ray radiation energy from laser produced polystyrene plasmas for shock ignition conditions. Physics of Plasmas, 2013, 20, 102702.	1.9	7
65	<mml:math <br="" xmlns:mml="http://www.w3.org/1998/Math/MathML">display="inline"&gt;<mml:mrow><mml:mi>K</mml:mi><mml:mi>L</mml:mi><mml:mi></mml:mi></mml:mrow> measurement for Li-like to O-like gold. Physical Review A, 2013, 88, .</mml:math>	:/mr <b>als</b> nath	1>dielectronic
66	A compact flat-response x-ray detector for the radiation flux in the range from 1.6 keV to 4.4 keV. Measurement Science and Technology, 2012, 23, 065902.	2.6	25
67	Study of x-ray radiant characteristics and thermal radiation redistribution in CH foam filling cylindrical cavities. Physics of Plasmas, 2011, 18, 042705.	1.9	11
68	Multiconfiguration Dirac-Fock calculations on multi-valence-electron systems: Benchmarks on Ga-like ions. Physical Review A, 2011, 84, .	2.5	25
69	Multiconfiguration Dirac-Fock results for forbidden transitions in the 2p 4 configuration. Open Physics, 2011, 9, .	1.7	7
70	Effects of valence-valence, core-valence and core-core correlations on the fine-structure energy levels in Zn-like ions. European Physical Journal D, 2011, 61, 15-20.	1.3	18
71	Beneficial effect of CH foam coating on x-ray emission from laser-irradiated high-Z material. Physics of Plasmas, 2011, 18, 053301.	1.9	19
72	Study on optimal inertial-confinement-fusion hohlraum wall radial density and wall loss. Physics of Plasmas, 2011, 18, 033301.	1.9	10

JIAMIN YANG

#	Article	IF	CITATIONS
73	Two-tracer spectroscopy diagnostics of temperature profile in the conduction layer of a laser-ablated plastic foil. Physics of Plasmas, 2010, 17, .	1.9	5
74	A novel flat-response x-ray detector in the photon energy range of 0.1–4 keV. Review of Scientific Instruments, 2010, 81, 073504.	1.3	98
75	Experimental study of the hydrodynamic trajectory of an x-ray-heated gold plasma. Physics of Plasmas, 2010, 17, .	1.9	8
76	High intensity x-ray line emission from aluminum plasmas generated by a 120TW, 30fs laser pulse. Physics of Plasmas, 2008, 15, 112704.	1.9	8